A 2D automatic converted-wave static-correction algorithm

Yimin Sun[1], Thierry Tonellot[2], Bahaaeldin Kamel[3], and Andrey Bakulin[2]

Abstract

Although multicomponent data acquisition opens the door for sharper seismic images and more accurate subsurface characterization, it also brings many challenges into multicomponent data processing. Among these challenges, converted-wave (S-wave) static correction is significant. Due to the fact that the earth may have dramatically different velocity responses to P- and S-waves, P-wave statics and S-wave statics should be treated as two independent problems; as a result, approximating S-wave statics by a simple scaling of the P-wave statics is not a satisfying solution. A new automatic S-wave static-correction algorithm is proposed and has been successfully applied on a full-fold Arabian Gulf ocean-bottom-cable (OBC) data set with promising results.

Introduction

Multicomponent seismic data acquisition enables more comprehensive seismic wavefield recording than the traditional single-component technique. In seismic recording, many complex wave-conversion phenomena are observed, such as a downgoing P-wave being converted to an upgoing S-wave (PS), a downgoing P-wave first being converted to a head wave and then being converted to an upgoing S-wave (PPS), and so on (Tatham, 1982). In oil and gas exploration, converted waves generally refer to PS conversion (Stewart et al., 2002).

Although converted-wave seismic data is richer in information, processing such data is more challenging than processing PP data. More steps are needed for successful data processing, such as S-wave static corrections, common-conversion-point (CCP) binning, P-S velocity analysis, etc. S-wave statics are two to 10 times greater than the corresponding P-wave statics, and, unlike P-wave statics, S-wave velocities are not influenced by the water table (Cary and Eaton, 1993; Li et al., 2012). P-wave and S-wave statics, therefore, are partially independent, and, as a result, applying a simple scaling to the derived P-wave statics may not provide the best results.

S-wave static-correction methods belong to two categories: model-driven and data-driven. Model-driven S-wave static-correction methods are similar to the methods used for PP data. The S-wave velocity model has to be derived first by certain methods, such as surface-wave inversion, refraction-wave analysis, or from uphole information (Schafer, 1991). Data-driven methods try to "honor the data" and usually strive to maximize the stacking power in the final image, with or without resorting to pilot traces (Schafer, 1991; Cary and Eaton, 1993).

In this paper, we propose a new automatic converted-wave static-correction method, which also belongs to the data-driven family. Our method consists of two phases. In phase 1, the seed statics are derived from the low-frequency components of the data, and the event structure of interest is determined from the aligned low-frequency events. In phase 2, with the seed statics as the initial values and with the event structure as the optimization guide, the stack power is further maximized on the original full-bandwidth data to obtain the final statics.

The automatic converted-wave static-correction algorithm

Similar to most data-driven static-correction methods, maximizing the stack power in the final image is used as the fitness function in our algorithm. Subsequently, the biggest challenge of this stack power maximization lies in correct determination of the time structure of events of interest. This is also the common bottleneck for automation where manual intervention is needed. To overcome this hurdle, we design our algorithm in a two-phase manner; the workflow of our method is shown in Figure 1. Consequently, for our algorithm to work correctly, the input data first must be properly preprocessed, including proper denoising, PS normal moveout (NMO) correction, application of P-wave statics, and CCP binning. In this paper, we assume that all these steps have been done correctly.

Phase 1 of the new algorithm comprises three steps: low-frequency signal extraction, seed-statics calculation, and time-structure determination. Long wavelength components have less resolution capability but more general structure recognition capability, so low-frequency components are a nice tool for us to figure out the time structure. As a result, in our workflow, low-frequency signals first are extracted from the original broadband data set for alignment. The choice of events of interest normally is based on geologic information, and, although we might not know exactly

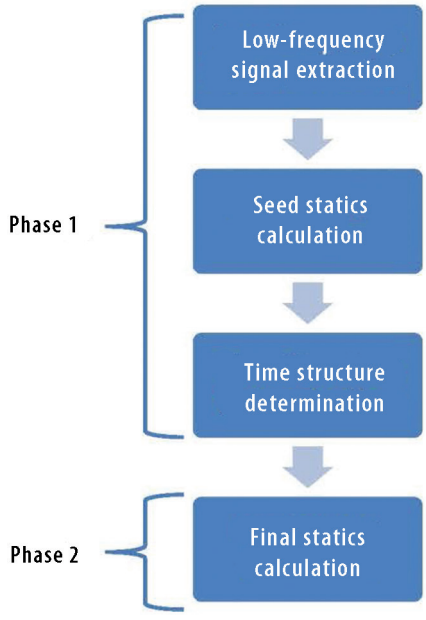

Figure 1. Workflow of the proposed automatic converted-wave static-correction algorithm.

[1]EXPEC ARC GRC Delft, Aramco Overseas Company BV.
[2]EXPEC Advanced Research Center, Saudi Aramco.
[3]GDPD, Saudi Aramco.

http://dx.doi.org/10.1190/tle35030280.1.

what the detailed time structure should be, we know that generally it should be spatially coherent. With this information, we resort to local coherence to align these low-frequency events. Local coherence means that, within a limited spatial area, events should be similar. A fitness function based on this is written as:

$$fitness_{seed} = \sum_{i=1,step=M/2}^{N} \sum_{t=T_1}^{T_2} \left\{ \sum_{j=i}^{i+M} f_j(t) \right\}^2, \quad (1)$$

where $f_j(t)$ is the stacked CCP trace (CCP No. = j), time range $[T_1, T_2]$ defines the zone of interest, iteration step i scans through the whole CCP number range in the dataset, M is the local coherence window size (how many consecutive CCPs), and iteration j covers the local coherence window starting from CCP i. Note that for iteration i, the increment step is $M/2$, which means a half window overlapping between consecutive local coherence windows. The definition of $f(t)$ is:

$$f_i(t) = \sum_j P_j[t - stat_{seed}(x)], \quad (2)$$

where $P(t)$ is a trace in the current CCP gather i, j iterates all traces in the CCP gather i, and $stat_{seed}(x)$ are the seed statics at surface location x for the low-frequency components.

We decide to use an advanced genetic algorithm (GA) (Sun and Verschuur, 2014) to maximize equation 1 because GA is a global search method unaffected by cycle skipping, and it can be automated once all parameters are carefully selected. The seed statics obtained from this step are used as the initial values for phase 2.

After the low-frequency components are aligned, the time structure must be determined to guide the optimization in phase 2. We first track central positions of one aligned event as the initial structure. In reality, signal-to-noise ratio prevents perfect alignment, so, normally, some jitter exists after this tracking. The correct structure should be relatively smooth, so some smoothing might have to be carried out. We propose to use a multiround median filtering procedure with a similar spatial window as the local coherence window, and the smoothed time structure then is used in phase 2.

After seed statics and time structure are available, we return to the original broadband data to further maximize the stacking power. With the obtained time structure as the optimization guide, now the fitness function (stacking power) is defined as:

$$fitness_{final} = \sum_{i=1,step=M/2}^{N} \sum_{t=T_1(j)}^{T_2(j)} \left\{ \sum_{j=i}^{i+M} f_j(t) \right\}^2, \quad (3)$$

$$f_i(t) = \sum_j P_j[t - stat_{final}(x)]. \quad (4)$$

In equation 3, time range $[T_1(j), T_2(j)]$ is defined by the determined time structure from phase 1, which is CCP-number dependent, iteration i scans through all the CCP numbers, M is the local coherence window size, and iteration j covers the local coherence window starting from CCP i. In equation 4, j covers all traces in CCP gather i, and $stat_{final}(x)$ are the final statics at surface location x.

Similar to equation 1, equation 3 is also highly nonlinear and can be solved naturally via the GA as well. Subsequently, considering that seed statics, which can be used as initial values, are already available from phase 1 and global search methods are far slower than local search methods, in phase 2 a local search algorithm is preferred. Due to the complexity of equation 3, derivative-based methods are not suitable here because there is no guarantee that it is a smooth function. As a result, direct search methods, in which no derivative information is needed at all, should be more suitable. After some tests, the back-and-forth scheme coordinate descent method (Nocedal and Wright, 1999) was chosen. This scheme not only best exploits the initial values but also provides fast convergence toward the final statics solution for the original broadband data set.

A 2D OBC field data example

Here we use an OBC field data set to demonstrate our proposed algorithm. The data set was acquired with a 10 km long receiver cable and two source lines. There are 200 receivers on the cable, each spaced 50 m apart. The time sampling rate of this data set is 4 ms, and the CCP bin size is 12.5 m. Due to the combined effect of severe lateral-velocity variations and low-velocity layer thickness variations below the seabed, this survey faces a tough near-surface challenge, both for P-wave and S-wave processing. P-wave statics, or source-side statics, have been obtained via refraction tomography and applied onto the data set, so the only outstanding statics issue for PS processing is the S-wave statics, or receiver-side statics. NMO velocities applied to this PS dataset are estimated from the PP NMO velocities by semblance-based gamma (V_P/V_S ratio) value picking (Grandi et al., 2005). The original image after CCP stacking without S-wave statics correction is shown in Figure 2, and near-surface S-wave static anomalies are clearly visible on reflections (at ~ 0.6 s in Figure 2), especially between CCP numbers 100 and 300. For our algorithm, the events of interest are between 0.3 s and 0.8 s.

We first low-pass filter the data set using 10 Hz as the upper frequency limit. The CCP stack of the low-frequency component

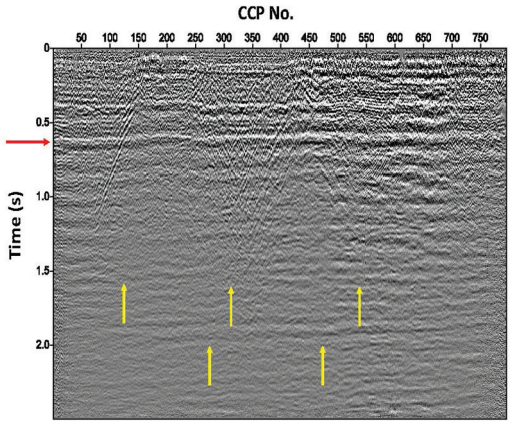

Figure 2. The original image after CCP stacking without S-wave statics correction.

is shown in Figure 3. For the events of interest between 0.3 s and 0.8 s, discontinuities are easy to observe. Using the advanced GA to optimize equation 1, seed statics are estimated, and the CCP stack of the aligned low-frequency data is shown in Figure 4a.

In the next step, the time structure of the events of interest will be estimated automatically by our structure-determination algorithm from the aligned low-frequency data. A particular event is first specified for the structure-determination algorithm to work on, which is the event between 0.55 s and 0.70 s, as indicated by the red arrow in Figure 2. Even after low-pass filtering, the corresponding event is still visible in the same time window, as shown in Figures 3 and 4a. The automatically determined event structure from the aligned low-frequency CCP stack image is shown in Figure 4b. The staircase effect is due to the fact that the signal is discreetly sampled at 4 ms intervals, and no interpolation is used here. This time structure is the smooth guide, which phase 2 needs.

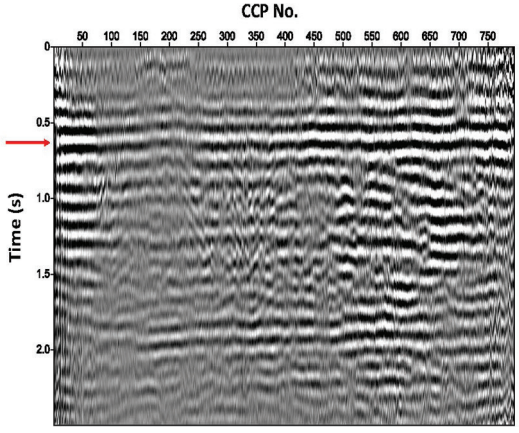

Figure 3. CCP stack of the low-frequency (10 Hz and below) components in the original data set without S-wave statics correction.

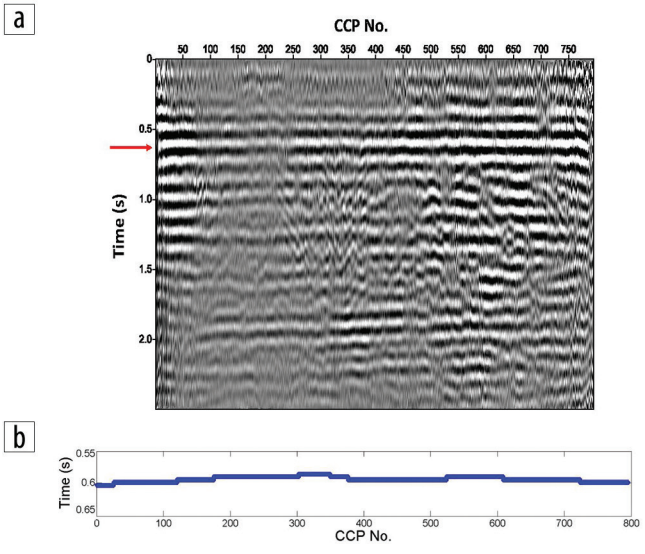

Figure 4. (a) CCP stack of the low-frequency (10 Hz and below) components with the S-wave seed statics applied. (b) The automatically determined event structure for the event of interest, marked by red arrow in Figures 2, 3, and 4a.

Using seed statics as the initial values, in phase 2 the back-and-forth coordinate descent algorithm tries to further maximize the stack power, defined in equation 3, on the original broadband data set. The final aligned CCP stack image is shown in Figure 5. It shows much better event continuity, not only for those events used in our optimization, i.e., between 0.30 s and 0.80 s, but also for all the deep events, i.e., those below 1.0 s (yellow arrows in Figures 2 and 5).

A 3D Arabian Gulf OBC case study

Marine seismic data from the Arabian Gulf faces a very tough S-wave statics challenge due to strong lateral velocity variations along the seabed. Here we apply our new algorithm to a 3D field data set from this area. Since our current algorithm is designed for the 2D case, we treat this large 3D data set as a bunch of independent 2D receiver lines and then work on them independently, reconstructing the 3D solution from individual 2D lines. For this data set, all the necessary preprocessing steps have been taken care of, so the only outstanding issue is the S-wave statics. First, a control set of S-wave statics are generated by the traditional crosscorrelation method with the help of a pilot trace. This static correction is compared with our new correction on CCP stacks and prestack time migration results in Figures 6 and 7. It is clear that not only do our new S-wave statics make all the events smoother and more continuous, but the vertical resolution also is improved, suggesting that our new method is capable of providing statics that better correspond to the actual propagation effects.

The water-bottom depth in the survey area is shown in Figure 8. As mentioned in the previous section, although it should be what is beneath the water bottom that finally determines the S-wave statics, it is expected that the S-wave statics may be influenced by the water-bottom topography. If we compare the S-wave statics estimated by crosscorrelation (Figure 9a) with the water depth, there is less correlation with the water-bottom topography than that from the newly estimated S-wave statics (Figure 9b), also suggesting that the latter results are more consistent with the propagation effects than conventional S-wave statics results.

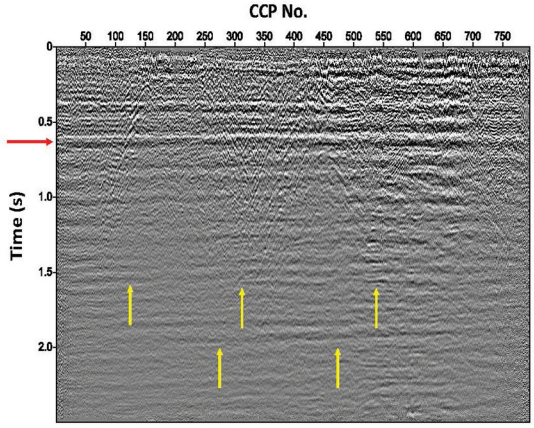

Figure 5. The final aligned CCP stack image with S-wave static-correction algorithm applied.

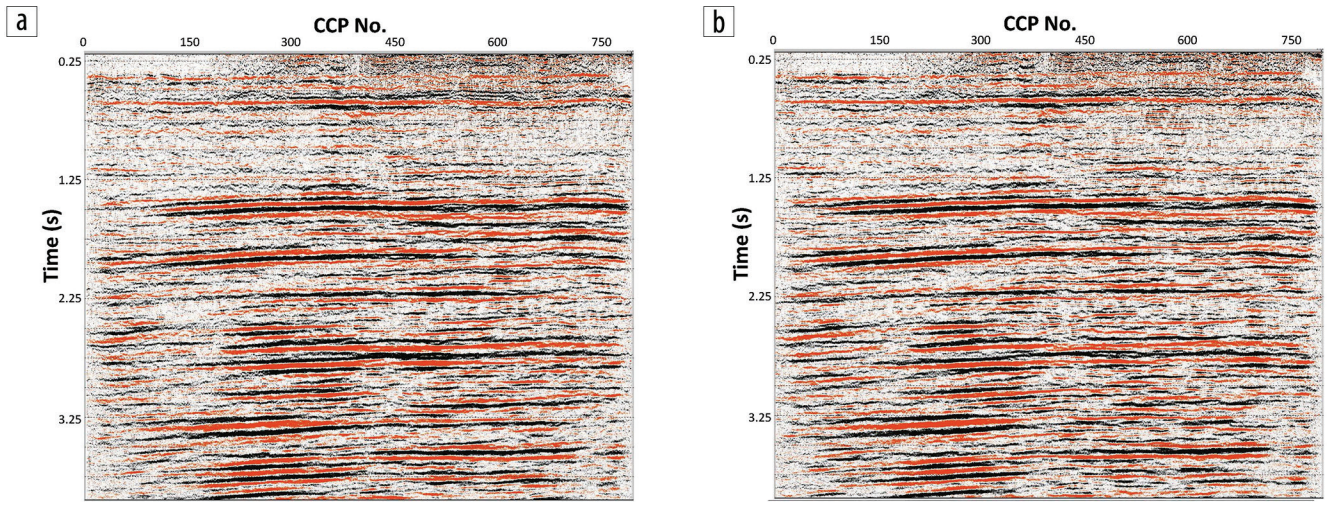

Figure 6. CCP stack comparison with (a) control S-wave statics applied and (b) newly estimated S-wave statics applied.

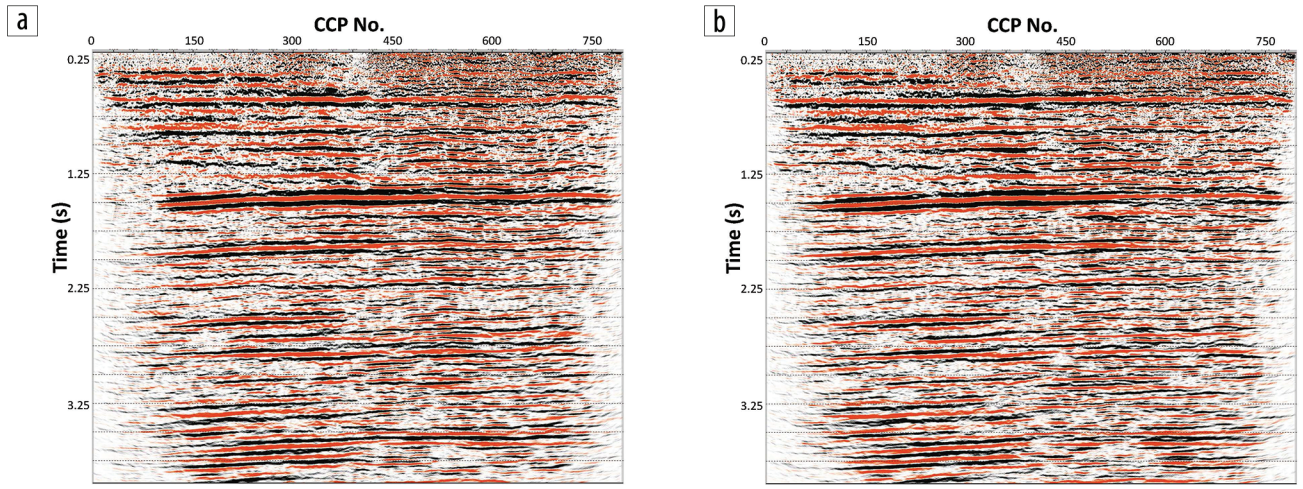

Figure 7. Prestack time migration comparison with (a) control S-wave statics applied and (b) newly estimated S-wave statics applied.

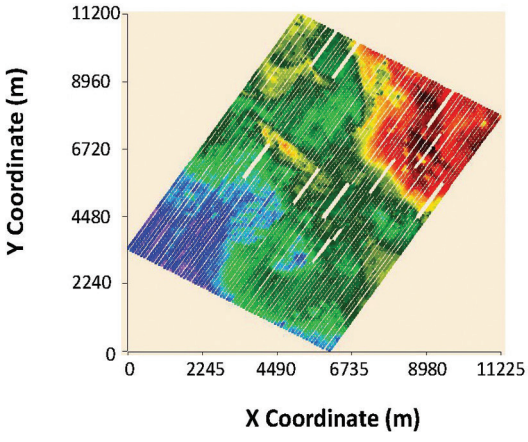

Figure 8. Water-bottom depth image of the survey area.

Conclusions

In this paper, we proposed a novel two-phase 2D automatic converted-wave static-correction algorithm. In phase 1, seed statics are estimated by an advanced GA on low-pass filtered data derived from the original broadband data set. The time structure of the events of interest is determined from the aligned low-frequency data. In phase 2, seed statics are used as the initial values, and the back-and-forth coordinate descent method is used to further maximize the stack power on the original broadband data set. We have applied this new algorithm successfully on an OBC field data set from the Arabian Gulf, and the results are promising. Generalization of the algorithm to 3D is straightforward and is currently under way. TLE

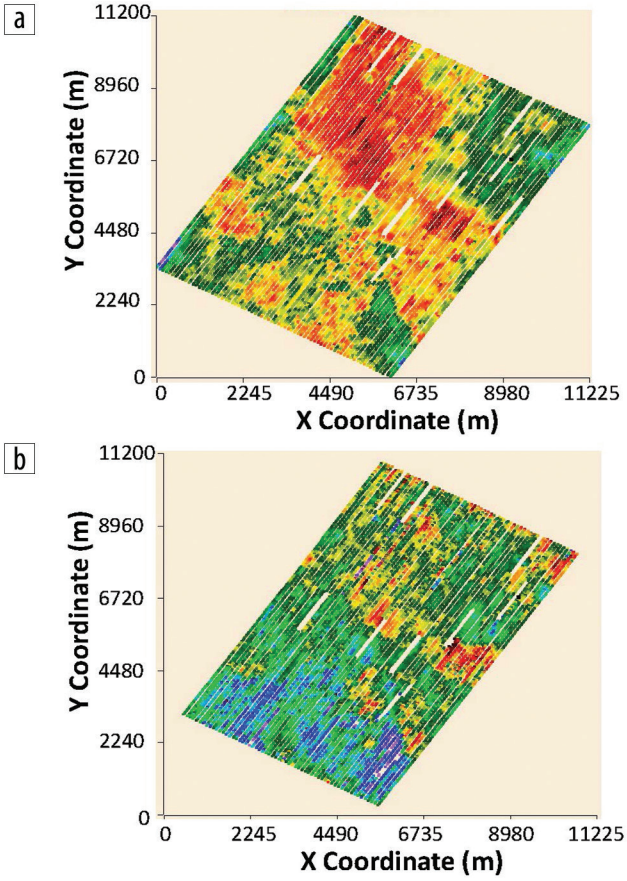

Figure 9. S-wave statics estimated by (a) the traditional method and (b) our new method.

Acknowledgments

The authors thank Michael Jervis for reviewing our manuscript and Saudi Aramco for permission to publish this paper.

Corresponding author: sun.delft@gmail.com

References

Cary, P. W., and D. W. S. Eaton, 1993, A simple method for resolving large converted-wave (P-SV) statics: Geophysics, **58**, no. 3, 429–433, http://dx.doi.org/10.1190/1.1443426.

Grandi, A., E. Stucchi, and A. Mazzotti, 2005, V_P / V_S ratios through multicomponent velocity analysis: 67th Conference and Exhibition, EAGE, Extended Abstracts, B024.

Li, Y. P., Z. T. Ma, P. Y. Sun, and H. S. Yang, 2012, Converted-wave static correction method for thick weathering area: Chinese Journal of Geophysics, **55**, no. 1, 76–83, http://dx.doi.org/10.1002/cjg2.1702.

Nocedal, J., and S. J. Wright, 1999, Numerical optimization: Springer.

Schafer, A.W., 1991. Converted-wave statics methods comparison, CREWES Report, 107–125.

Stewart, R. R., J. E. Gaiser, R. J. Brown, and D. C. Lawton, 2002, Converted-wave seismic exploration: Methods: Geophysics, **67**, no. 5, 1348–1363, http://dx.doi.org/10.1190/1.1512781.

Sun, Y., and D. J. Verschuur, 2014, A self-adjustable input genetic algorithm for the near-surface problem in Geophysics: IEEE Transactions on Evolutionary Computation, **18**, no. 3, 309–325, http://dx.doi.org/10.1109/TEVC.2013.2261075.

Tatham, R. T., 1982, Vp/Vs and lithology: Geophysics, **47**, no. 3, 336–344, http://dx.doi.org/10.1190/1.1441339.